Modeling of neutral beam injection in Tokamaks

BY YOUJUN HU

Institute of plasma physics, Chinese Academy of Sciences
Email: yjhu@ipp.cas.cn

Abstract

A numerical code modeling the deposition and collisional transport of neutral beam particles in Tokamaks is being developed. These notes discusses the physical models used in the code.

1 Neutral particle source

A Neutral Beam Injector (NBI) consists of (1) an ion source, which produces high-energy ions, (2) a neutralizing chamber, which neutralizes the high-energy ions, and (3) a bending magnetic system to remove remained charged particles from the beam. The ion source itself consists of an arc chamber, which produces low-energy ions, and a set of accelerating electrodes, which is attached to the window of the arc chamber, to accelerate the ions to high energy. An example of the configuration of accelerating electrodes is shown in Fig. 1.

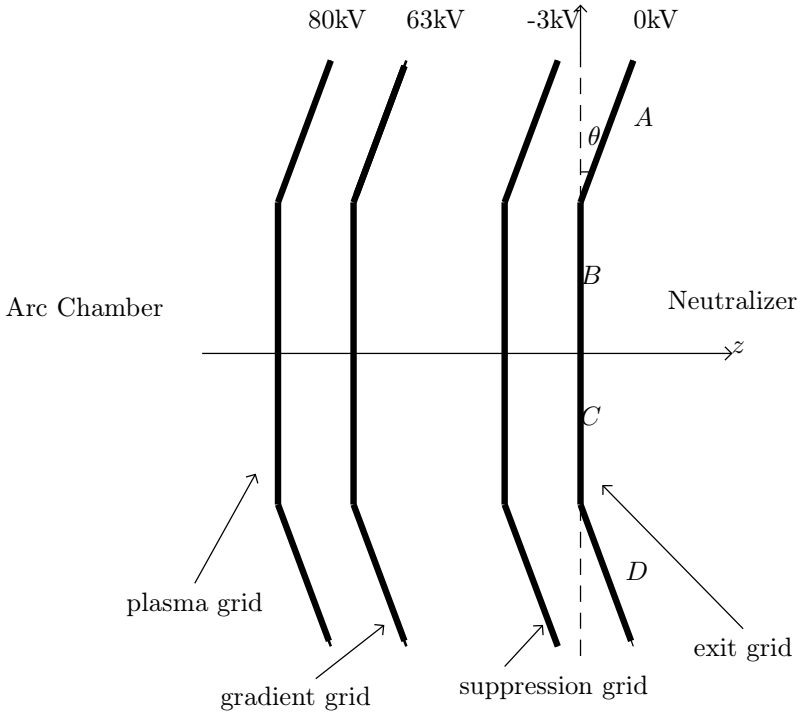

Figure 1. Four groups of accelerating electrode grids of the ion source of EAST neutral beam injector, which are called plasma grid, gradient grid, suppression grid, and exit grid, respectively. Every electrode grid have four sub-electrode, indicated by A, B, C, and D on the figure. Sub-electrodes A and D are rotated to the right with respect to the centeral sub-electordes B and C by a small angle $\theta = \left(1\frac{1}{12}\right)$degree. This angle is exaggerated on the figure.

1.1 Focal length of beam

The central beam from each of the four sub-electrodes is perpendicular to the corresponding grid plane. As is shown in Fig. 1, two of the sub-electrodes A and D are rotated to the right with respect to the centeral sub-electordes by a small angle θ. This focuses the central beams from A and D with a focal length given by

$$f_b \approx \frac{2y_0}{\tan(2\theta/3)}, \tag{1}$$

where y_0 is the vertical half-width of the sub-electrode, as shown in Fig. 2. [Proof of Eq. (1): Using the geometry given in Fig. 2, we have $\alpha_1 + \alpha_2 = \theta$ and $\sin\alpha_1 = 2\sin\alpha_2$. Since θ is small, both α_1 and α_2 are small. Thus we have the approximation $\sin\alpha_1 \approx \alpha_1$ and $\sin\alpha_2 = \alpha_2$. Using these, we obtain $\alpha_1 = 2\theta/3$. The focal length is then written as $f_b = 2y_0/\tan(\alpha_1) = 2y_0/\tan(2\theta/3)$.] For $\theta = \left(1\frac{1}{12}\right)$degree, Eq. (1) gives $f_b = 9.5194m$.

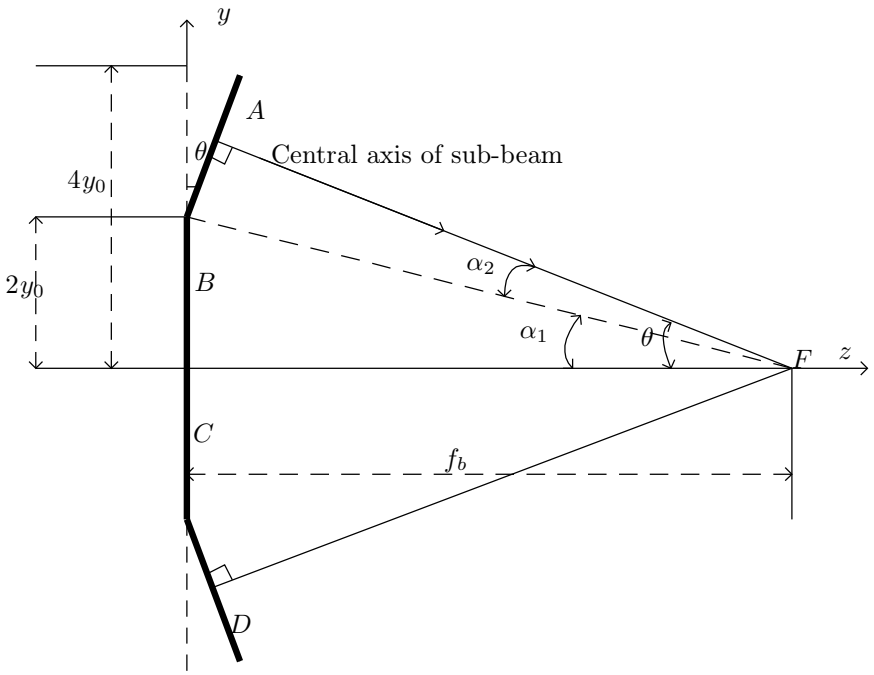

Figure 2. Geometry of exit electrode of the ion source of EAST neutral beam injector. The electrode has four sub-electrodes, indicated by A, B, C, and D on the figure. The width of each sub-electrode is $2y_0$ with $y_0 = 0.06m$. Sub-electrodes A and D are rotated to the right with respect to the centeral sub-electordes B and C by a small angle $\theta = \left(1\frac{1}{12}\right)$degree. The central axis of the two sub-beams (beams from electrode A and D) intersect at F. The vertical focal length f_b is defined as the distance from point F to the electrode BC plane.

The above focal length is for the focus in the vertical direction. The horizontal focal length is infinity for EAST NBI because all the sub-electrodes are flat along the horizontal direction.

2 Beam attenuation in plasma

When a neutral beam goes through a tokamak plasma, along the trajectory of the beam, the beam intensity is attenuated due to the ionization of neutral particles by the background plasma. The attenuation of beam intensity can be modeled by the following differential equation:

$$\frac{dI}{dl} = -\nu(l) I, \tag{2}$$

where $I(l) = n_b(l) v_b$ is the beam intensity, n_b is the number of beam particles per unit length along the beam trajectory (straight line) and v_b their velocity (assumed to be constant along the trajectory), and $\nu(l)$ is given by

$$\nu(l) = n_i \sigma_{\text{ch}} + n_i \sigma_i + n_e \frac{\langle \sigma_e v_e \rangle}{v_b} \tag{3}$$

where σ_{ch} is the cross-section for charge exchange with plasma ions, σ_i are the cross-section for ionization by plasma ions, $\langle \sigma_e v_e \rangle$ is the electron impact ionization rate coefficient averaged over the Maxwellian distribution ($\langle \sigma_e v_e \rangle / v_b$ is the effective cross-section of electron impact ionization). The dependence of these cross-sections on the energy of beam particles was given in Fig. 5.3.1 of Wesson's book "Tokamaks" (for reference ease, this figure is included in Appendix A of this report (Fig. 27)). Next section presents the data for the cross-sections I obtain by reading relevant references.

2.1 Ionization cross-sections

It took me some time to try to find up-to-date data for the various ionization cross-sections. I have browsed the data in the ADAS data base, which is said to include the most comprehensive and accurate data for the various atom processes in fusion plasmas. However, it seems to me that some basic information is still lacking in ADAS and some information may be inaccurate or confusing (at lest to me). One example is shown in Fig. 3, where I found the charge-exchange cross-section given in ADAS is too big to be reasonable.

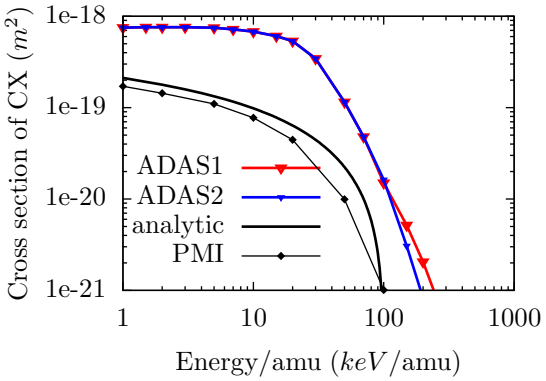

Figure 3. Cross section of charge exchange between Hydrogen-Hydrogen (including the isotopes ^1H, ^2H, and ^3H) as a function of the kinetic energy per amu (atom mass unit). The data indicated by the blue line and red line are from the ADAS data files "qcx#h0_e2p#h1.dat" and "qcx#h0_e2s#h1.dat", respectively. The results labeled by "PMI" is from the data on Page 78 of Ref. [2]. The analytic fitting results (black line) are from Eq. (28) of Ref. [1], which is given by $\sigma_{ex}(m^2) = 10^{-18}(1-0.5(2E)^{0.06} + 4\times10^{-7}E)$, where E is the collision energy per amu in eV/amu. The values of the fitting cross section agrees with those given in Fig. 5.3.1 of Wesson's book (Fig. 27 of this report) and these results are almost one order smaller than the results given by ADAS (Presently I do not know the reason. Numerical teasing indicates neutral beams will deposit at the pedestal of EAST if the ADAS cross section is used, which indicates that ADAS cross section is too big to be reasonable).

I can not find the data of the ion impaction ionization cross section from the ADAS database. It seems that there are very few papers discussing the ion impaction ionization cross section. One of the papers I found useful is Kaganovich's paper[3], which gives the following fitting formula for the impaction ionization cross section by a fully stripped ion, σ_i:

$$\sigma_i(v, I_{\rm nl}, Z_p) = \pi a_0^2 \frac{N_{\rm nl} Z_p^2}{(Z_p+1)} \frac{E_0^2}{I_{\rm nl}^2} G^{\rm new}\left(\frac{v}{v_{\rm nl}\sqrt{Z_p+1}}\right), \tag{4}$$

where v is the relative velocity between the atom and the ion, Z_p is the atomic number of the fully stripped ion, $I_{\rm nl}$ is the ionization potential of the atom, $v_{\rm nl} = v_0\sqrt{2I_{\rm nl}/E_0}$ with $v_0 = 2.2\times10^6 m/s$ and $E_0 = 27.2$eV, $N_{\rm nl}$ is the number of electrons in the nl orbital of the atom ($N_{\rm nl}=1$ for hydrogen), $a_0 = 0.529\times10^{-10}m$ is the Bohr radius, and

$$G^{\rm new} = \frac{1}{x^2}\exp\left(-\frac{1}{x^2}\right)[1.26 + 0.283\ln(2x^2+25)]. \tag{5}$$

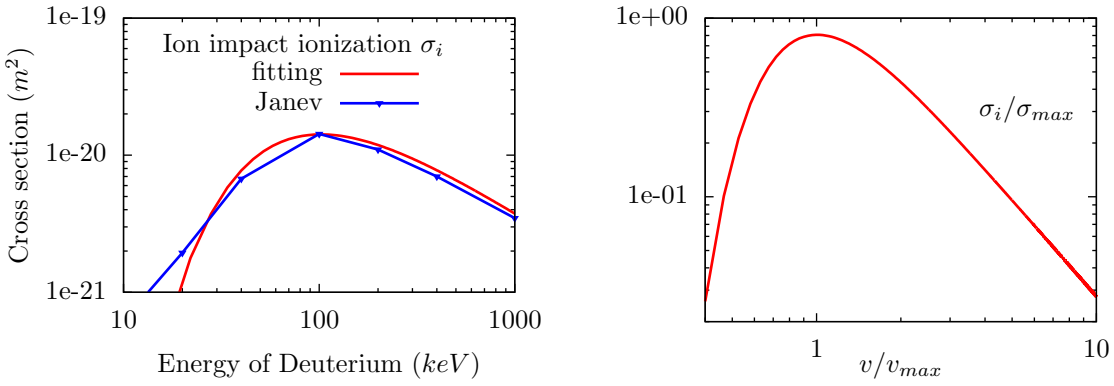

Figure 4. Left: Cross section of ion impact ionization of deuterium as a function of the kinetic energy of deuterium atom (red line is calculated by using Eq.(4), data of blue line are from the data on Page 68 of Ref. [2]). Right: Normalized cross section $\sigma_i\,/\,\sigma_{\rm max}$ as a function of the normalized velocity $v\,/\,v_{\rm max}$, where $\sigma_{\rm max} = \pi a_0^2 Z_p^2\,/\,(Z_p+1)E_0^2\,/\,I_{\rm nl}^2$, $v_{\rm max} = v_{nl}\sqrt{Z_p+1}$. These results agree with Fig. 3 of Kaganovich's paper[3].

For neutral beam injection relevant to present tokamaks, the thermal velocity of plasma ions are much smaller than the velocity of beam atoms, i.e., $v_{ti} \ll v_b$, so that $v_{ti} \approx 0$ can be assumed. As a result, $\sigma_{\rm ch}$ and σ_i discussed above are independent of the temperature of the background plasma ions. However, the electron impact ionization rate coefficient $\langle \sigma_e v_e \rangle$ usually depends on the temperature of background electrons because the thermal velocity of electrons is usually comparable to the beam velocity and an averaging over the electron Maxwellian distribution is needed. The dependence of the electron ionization rate coefficient $\langle \sigma_e v_e \rangle$ on the electron temperature is plotted in Fig. 5.

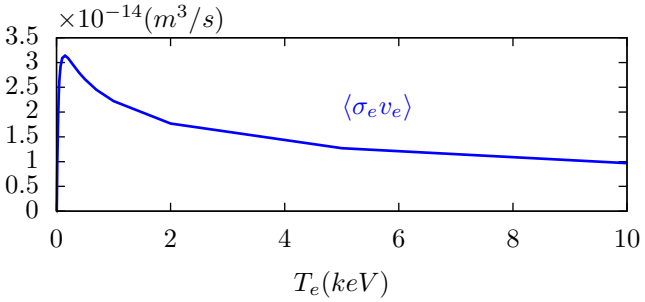

Figure 5. The dependence of the electron impact ionization rate coefficient $\langle \sigma_e v_e \rangle$ on the electron temperature T_e. These data are obtained by using the open-ADAS reading program "xxdata_07" to acces the ADAS data file "szd93#h_h0.dat", which stores the electron ionization rate coefficient for hydrogen atom.

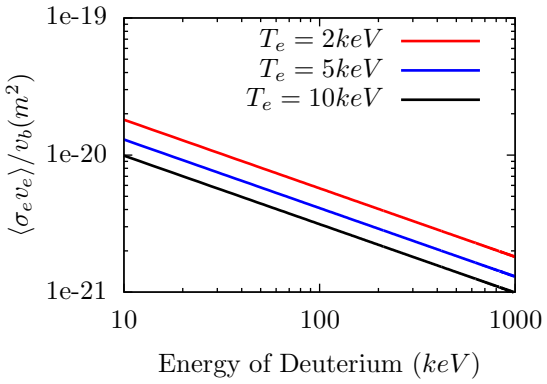

Figure 6. The dependence of the electron impact ionization cross section $\langle \sigma_e v_e \rangle / v_b$ on the kinetic energy of the Deuterium atom for the three cases with $T_e = 2$keV, 5keV, and 10keV.

Presently, multi-step ionization processes are not incorporated in my code. Ionization cross section due to the contribution of impurity ions are also not included.

2.2 Monte-Carlo implementation of beam attenuation (fast ions generation)

The solution to Eq. (2) can be analytically obtained, which is given by

$$I = I_0 e^{-\int_0^l \nu(l')dl'}, \tag{6}$$

where I_0 is the beam density at the starting point of the beam trajectory. The solution (6) indicates an exponential attenuation of the beam intensity along the beam trajectory.

The Mote-Carlo method of implementing the beam attenuation due to ionization process is as follows. First load assemble of neutral particles with each particle associated with a uniform random number η in the range of $[0, 1]$. Along the trajectory of each neutral particle (straight line), the integration $s = \int_0^l \nu(l')dl'$ is calculated to examine whether $s \geqslant \ln(1/\eta)$ or not. If $s \geqslant \ln(1/\eta)$, then the neutral particle is considered to be ionized. A simple numerical experiment can verify that this implementation generate results in agreement with the analytic solution given by Eq. (6).

Those neutral particles that are not yet ionized when they reach the inner wall of the device are usually lost to the wall and this loss of neutral particles are called shine-through loss. The shine-through loss is usually very small on large machine like ITER but for a medium-size tokamak like EAST, shine-through loss can be large, especially for the more perpendicular beam and lower-density plasmas.

To represent the neutral particles source from the injector, an assemble of neutral particles are loaded with desired distribution over energy and direction of velocity. In my present implementation of the source in the code, all the particles from the source has the same direction of velocity (i.e., beam divergence is neglected) but with different tangency radius. Due to the presence of dual-atom and tri-atom molecules in the accelerator, single-atom neutral particles injected into tokamaks have three possible energies E, $E/2$ and $E/3$. Energy distribution over these three energies is implemented. The spatial distribution of neutral particles on the injector surface are also implemented by assuming a bi-gaussian distribution along the vertical and horizontal directions (check, density vs. intensity).

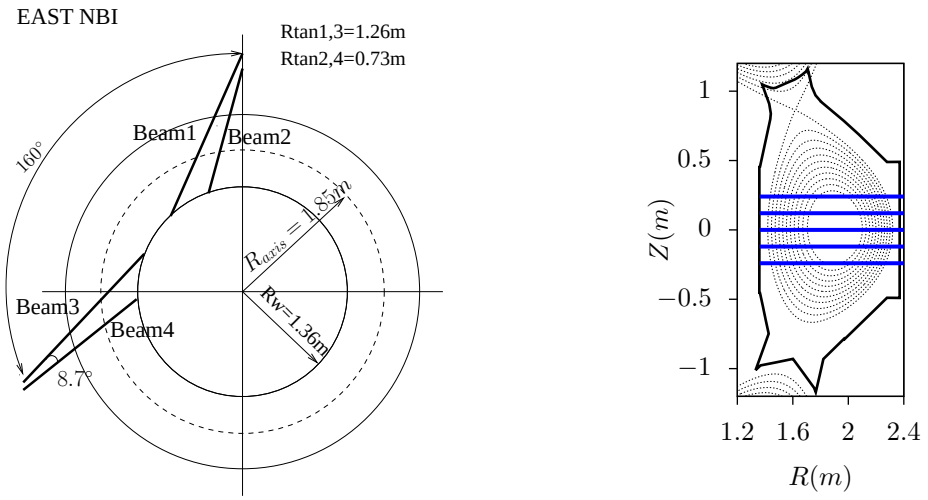

Figure 7. Top view (left) and poloidal view (right) of neutral beam lines on EAST.

The injector port on EAST is rectangular with heigh of 0.12m and width of 0.48m. The number ratio between particles with full-energy, half-energy and third energy is $n_f/n_{f/2}/n_{f/3} = 80:14:6$.

3 Numerical results

3.1 Equilibrium profiles

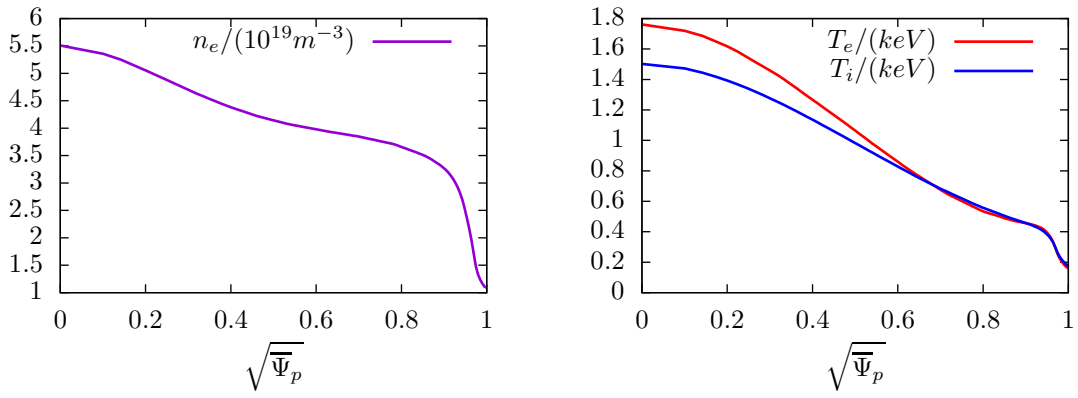

Figure 8. Profiles of number density of electrons (left) and temperature of electrons and ions (right) of EAST discharge #62585@2.8s.

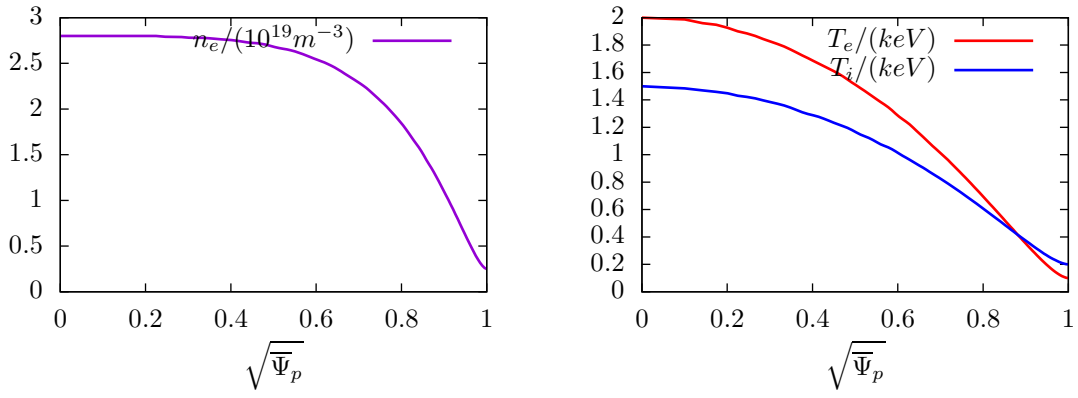

Figure 9. Profiles of number density of electrons (left) and temperature of electrons and ions (right) of EAST discharge #59954@3.2s

3.2 Spatial distribution of fast ions generated by neutral beam injection

The shine-through time of a neutral particle ($4 \times 10^{-7}s$ for 50keV neutral beam on EAST) is much shorter than the typical poloidal orbit period ($\sim 4 \times 10^{-5}s$). Therefore the time difference between the birth of various fast ions is tiny and thus can be neglected, i.e., all the fast ions can be considered to be born at the same time.

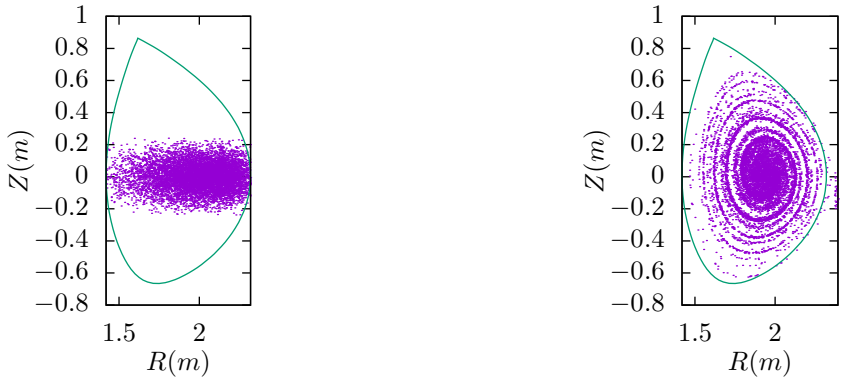

Figure 10. Poloidal view of the locations of fast ions at birth (left) and 0.078ms later (right) due to neutral beam particles of 50keV injected to EAST tokamak from a rectangular source with heigh of 0.12m and width of 0.48m. The tangency radius of the central beam of the source is $0.73m$. The central beam is on the midplane and the divergence of the beams is neglected. Magnetic configuration is from EAST discharge #62585@2.8s (gfile provided by ZhengZheng). The electron density profile is plotted in Fig. 8.

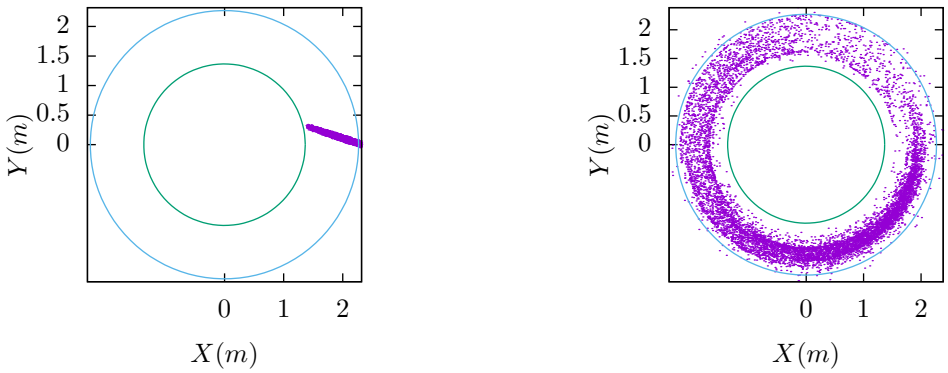

Figure 11. Top view of the locations of fast ions at birth (left) and 0.078ms later (right) due to neutral beam particles of 50keV injected to EAST tokamak from a rectangular source with heigh of 0.12m and width of 0.48m. The tangency radius of the central beam of the source is $0.73m$. The central beam is on the midplane and the divergence of the beams is neglected. Magnetic configuration is from EAST discharge #62585@2.8s (gfile provided by ZhengZheng).

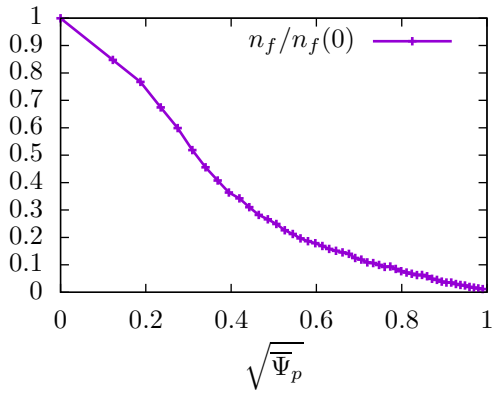

Figure 12. Density profiles of initially deposited NBI fast ions.

3.3 Loss of fast ions to the wall

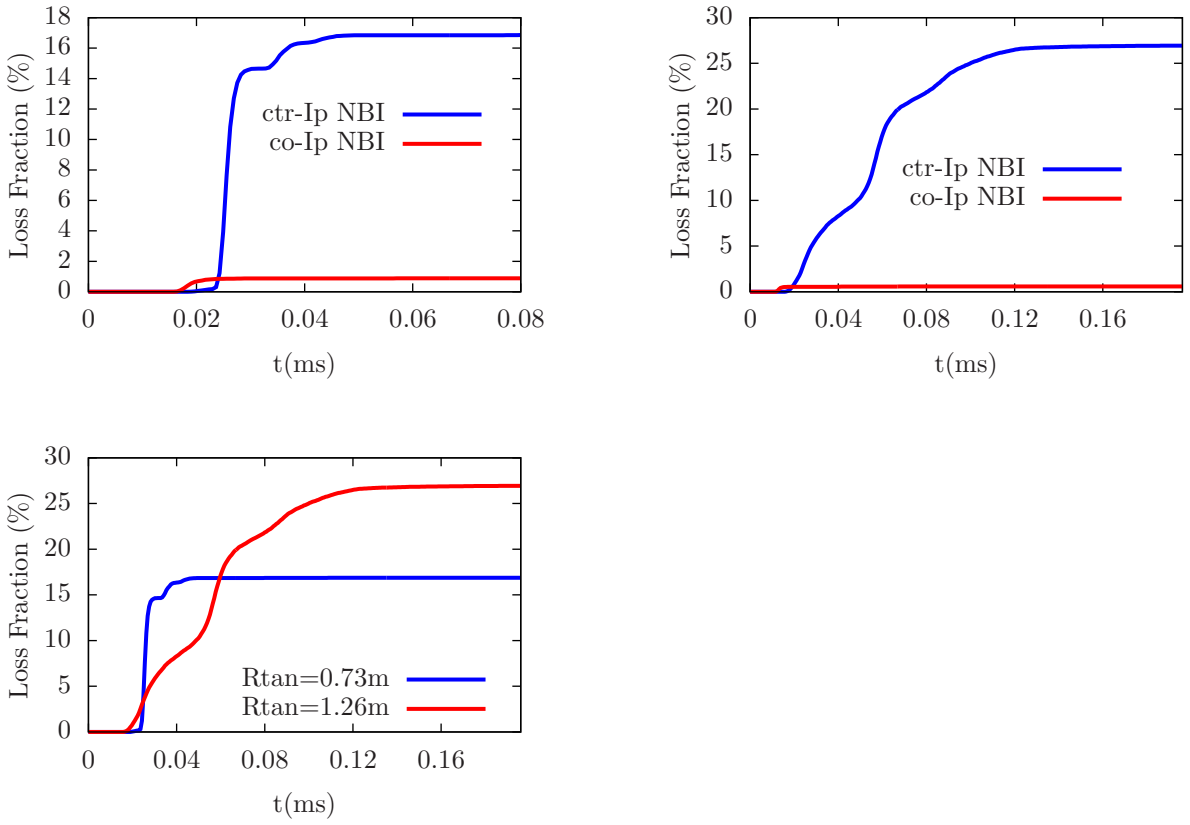

Figure 13. Comparison of fast ions loss fraction due to counter-current NBI and co-current NBI in EAST discharge #62585@2.8s. Maximal energy is 50keV. The central beam is on the midplane with the tangency radius being $0.73m$ (left figure) and $1.26m$ (right figure).

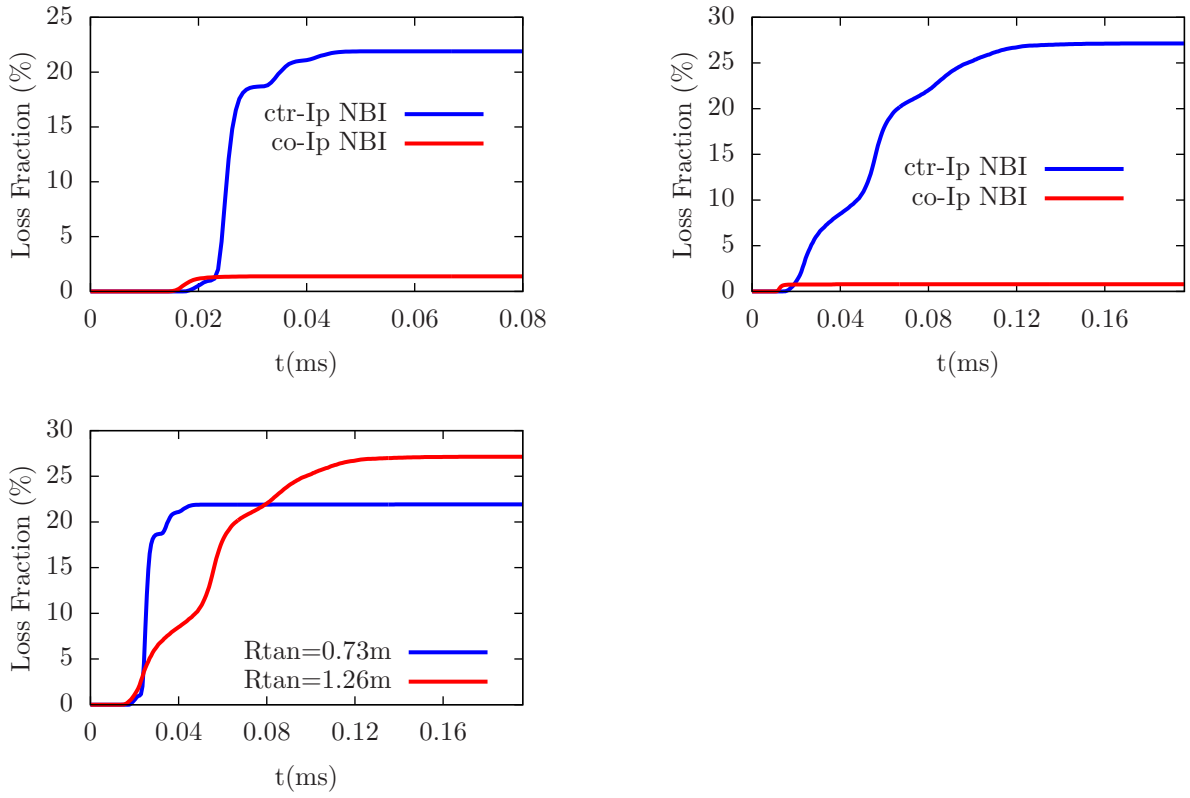

Figure 14. The same as Fig. 13 but with FLR effect included.in EAST discharge #62585@2.8s.

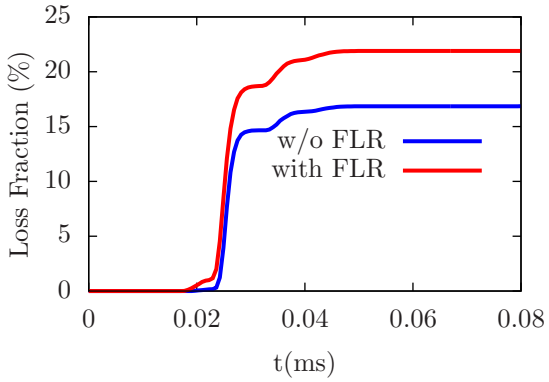

Figure 15. Rtan=0.73m. cntr-Ip. in EAST discharge #62585@2.8s.

⟨image|/home/yj/theory/nbi/fig7/p.eps||||⟩

Figure 16. Comparison of fast ions prompt loss fraction in EAST discharge #62585@2.8s. Maximal energy is 50keV. The central beam is on the midplane with the tangency radius being $0.73m$. LCFS is used as the loss boundary

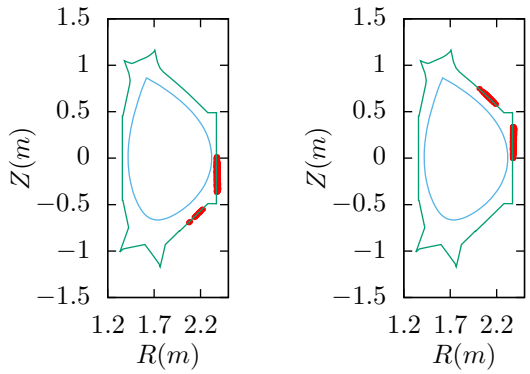

Figure 17. Distribution of the lost fast ions on the first wall for the case $B_\phi < 0$ (left) and $B_\phi > 0$ (right). Neutral beam is injected in $+\hat{\phi}$ direction, which is in the counter-current injection. The magnetic configuration is from EAST discharge #62585@2.8s (gfile provided by ZhengZheng).

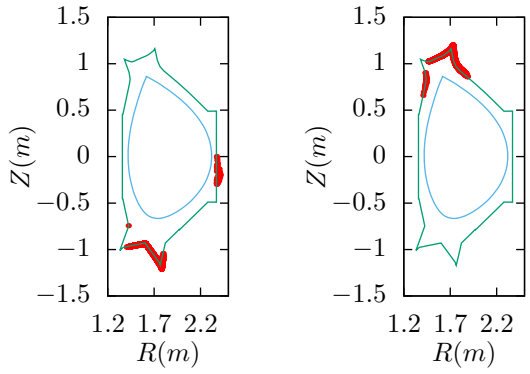

Figure 18. Rtan=1.26m

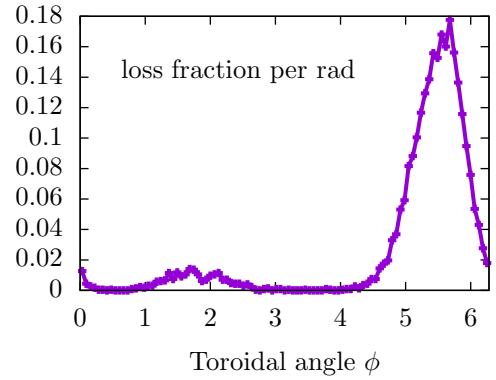

Figure 19. Toroidal distribution of lost fast ions

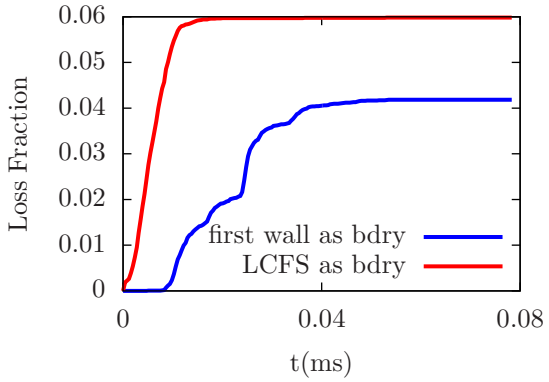

Figure 20. Comparison of fast ions loss fraction due to counter-current neutral beam injection in EAST discharge #62585@2.8s calculated using (a) the first wall of the machine and (b) the last-closed-flux-surface (LCFS) as the loss boundary.

4 Effects of RMP on confinement of NBI fast ions

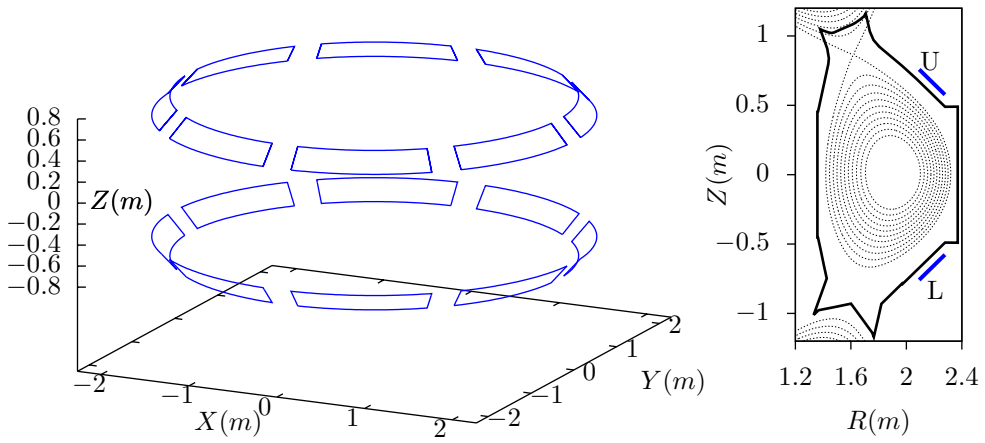

Figure 21. Location of the RMP coils on EAST tokamak in 3D view (left) and poloidal view (right).

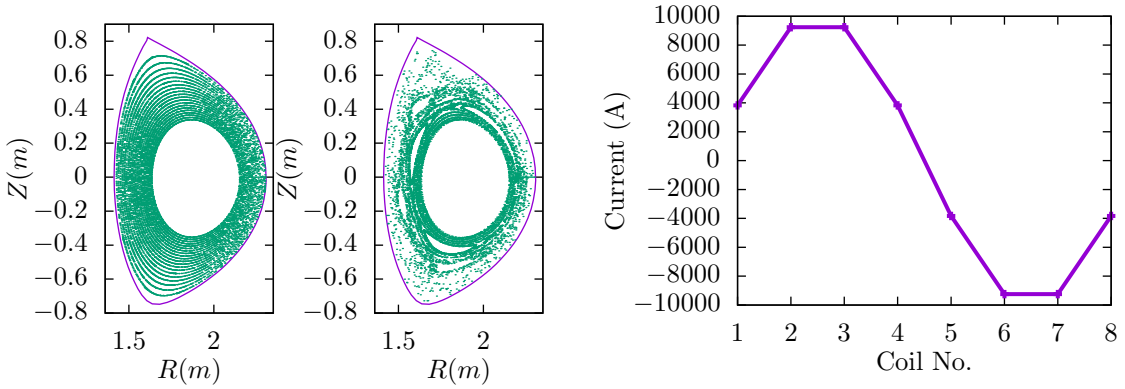

Figure 22. Poincare section of magnetic field lines of axisymmetric magnetic field (left) and the superpostion of the axisymmetric magnetic field and a magnetic perturbation generated by RMP coils (middle). Right: current in each RMP coil. The axisymmetric magnetic field is from EAST discharge #59954@3.1s. These Poincare sections are obtained by tracing 20 field lines starting from 20 points on the the low-field-side midplane, and then then recording the intersecting points of these field lines with the $\phi = 0$ plane. The maximum number of intersecting points for each field line is set to 700. In (a), i.e. axisymetrica field, the Poincare points form nested surface, which inidcates the accuracy of the field line tracing is good. In (b), some field lines touch the first wall of the machine before they finish 700 toroidal turns.

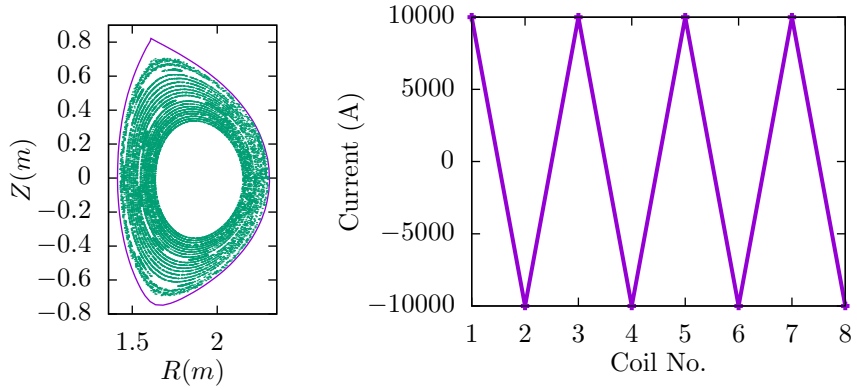

Figure 23. Left: Poincare section of magnetic field lines. Right: current in each upper-RMP coils (the current in lower-RMP coils are identical with that of the corresponding upper coil).

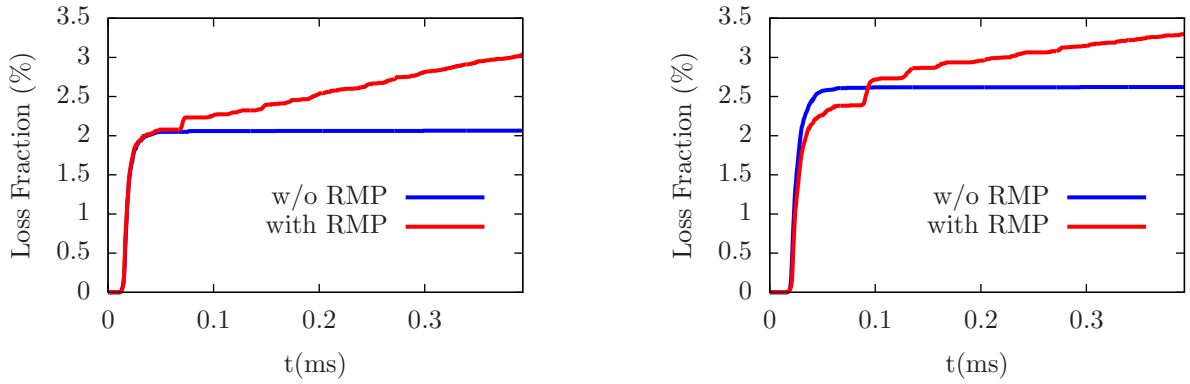

Figure 24. (1)Rtan=1.264m, (2) Rtan=0.731, co-Ip, in EAST discharge #59954@3.2s

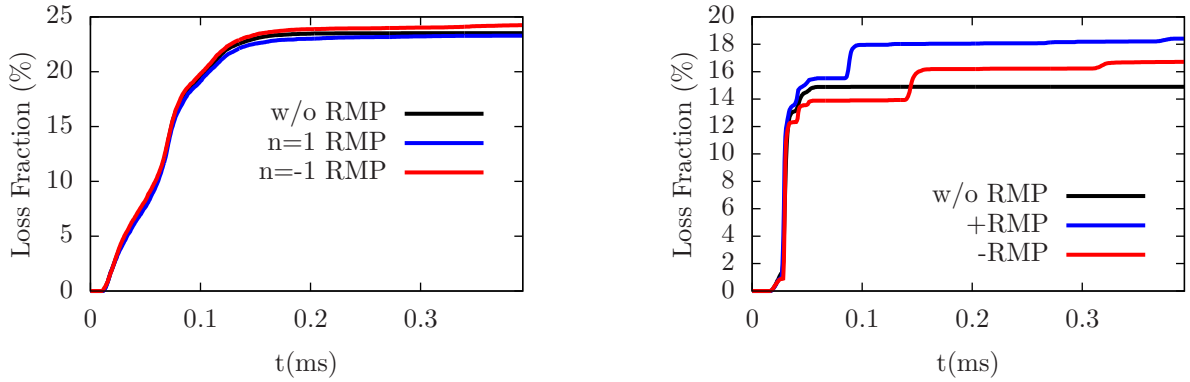

Figure 25. (1)Rtan=1.414m (2) Rtan=0.606, cntr-Ip, in EAST discharge #59954@3.2s

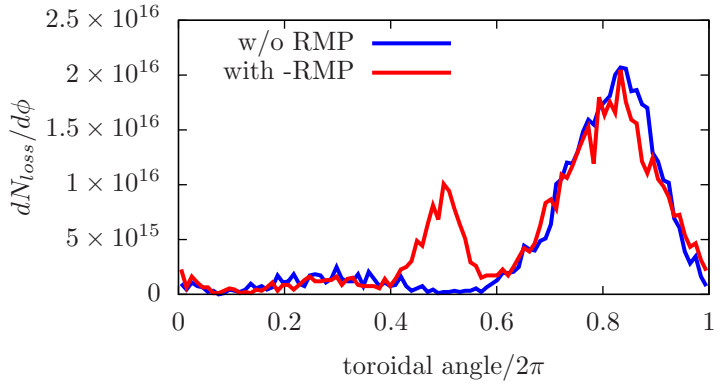

Figure 26. Rtan=0.606, cntr-Ip , in EAST discharge #59954@3.2s

4.1 Torque generated by beam

4.2 Current driven by beam

4.3 Collisions with Maxwellian background ions and electrons

4.3.1 Monte-Carlo implementation given in Z. Lin's paper[5]

Z. Lin's paper[5] provided a Monte-Carlo method of implementing the collision of a test particle with a Maxwellian background species, which is given by (how to derive these formula from a known collision operator?)

$$v_{\parallel} = v_{\parallel 0} - \nu_{s\parallel}\Delta t + \sqrt{12}(R_1 - 0.5)\sqrt{\nu_{\parallel}\Delta t}, \tag{7}$$

and

$$v_{\perp}^2 = v_{\perp 0}^2 - \nu_{s\perp}\Delta t + \sqrt{12}(R_2 - 0.5)\sqrt{\left(\nu_{\perp} - \frac{\nu_{\parallel\perp}^2}{\nu_{\parallel}}\right)\Delta t} + \sqrt{12}(R_1 - 0.5)\frac{\nu_{\parallel\perp}}{\nu_{\parallel}}\sqrt{\nu_{\parallel}\Delta t} \tag{8}$$

where R_1 and R_2 are two independent random numbers chosen from a uniform distribution from 0 to 1, Δt is the time step, $\nu_{s\parallel}$, $\nu_{s\perp}$, $\nu_{\parallel}$, $\nu_{\perp}$, and $\nu_{\parallel\perp}$ are given by

$$\nu_{s\parallel} = v_{\parallel}\left(1 + \frac{m_\alpha}{m_\beta}\right)F\nu_0, \tag{9}$$

$$\nu_{s\perp} = \left[2v_{\perp}^2\left(1 + \frac{m_\alpha}{m_\beta}\right)F - v_{\perp}^2 H - (2v_{\parallel}^2 + v_{\perp}^2)G\right]\nu_0, \tag{10}$$

$$\nu_{\parallel} = [v_{\parallel}^2 H + v_{\perp}^2 G]\nu_0, \tag{11}$$

$$\nu_{\perp} = [4v_{\perp}^2(v_{\perp}^2 H + v_{\parallel}^2 G)]\nu_0 \tag{12}$$

$$\nu_{\parallel\perp} = [2v_{\perp}^2 v_{\parallel}(H - G)]\nu_0, \tag{13}$$

with F, G, and H defined by

$$F = \phi(x), \tag{14}$$

$$G = \left(1 - \frac{1}{2x}\right)\phi(x) + \frac{d\phi(x)}{dx}, \tag{15}$$

$$H = \frac{1}{x}\phi(x), \tag{16}$$

where $x = v^2/v_{\mathrm{th}\beta}^2$ and $\phi(x)$ is the Maxwellian integral defined by

$$\phi(x) = \frac{2}{\sqrt{\pi}}\int_0^x e^{-t}\sqrt{t}dt,$$

which can be written in terms of the error function as (using software maxima)

$$\phi(x) = \frac{e^{-x}}{\sqrt{\pi}}[\sqrt{\pi}\mathrm{erf}(\sqrt{x})e^x - 2\sqrt{x}]. \tag{17}$$

The basic collision frequency ν_0 is defined by

$$\nu_0 = \frac{\Gamma^{\alpha/\beta}}{v^3} = \frac{n_\beta q_\alpha^2 q_\beta^2 \ln\Lambda^{\alpha/\beta}}{4\pi\varepsilon_0^2 m_\alpha^2 v^3}, \tag{18}$$

which is different from the formula given in Lin's paper[5] (it seems that Lin misused a formula of Gauss-unit in the paper that uses S.I units elsewhere).

The above formula can be applied to model collisions of fast particles with both ions and electrons.

4.3.2 Collision implemented in MEGA code [7]

A Monte-Carlo implementation of collision of fast ions with background electrons and ions are given in Todo's paper [7], where the pitch-angle variable $\lambda = v_\parallel / v$ and velocity v are altered at the end of each time step according to the following rules:

$$\lambda_{\text{new}} = \lambda_{\text{old}}(1 - 2\nu_d \Delta t) \pm \sqrt{(1-\lambda_{\text{old}}^2) 2\nu_d \Delta t}, \tag{19}$$

and

$$v_{\text{new}} = v_{\text{old}} - \nu_s \Delta t \left(v + \frac{v_c^3}{v^2} \right) + \frac{\nu_s \Delta t}{m_f v_{\text{old}}} \left[T_e - \frac{1}{2} T_i \left(\frac{v_c}{v_{\text{old}}} \right)^3 \right] \pm \sqrt{\frac{\nu_s \Delta t}{m_f} \left[T_e + T_i \left(\frac{v_c}{v_{\text{old}}} \right)^3 \right]}, \tag{20}$$

where $\pm$ denotes a randomly chosen sign with equal probability for plus and minus, Δt is the time step, ν_s is the slowing down rate given by $\nu_s = 1/t_s$ with the slowing down time t_s given by Eq. (36), ν_d is the pitch-angle scattering rate, which is given by

$$\nu_d = (1 + Z_{\text{eff}})\nu_0 = (1 + Z_{\text{eff}}) \frac{\Gamma^{\alpha/e}}{v^3} = \left(\frac{1 + Z_{\text{eff}}}{v^3} \right) \frac{n_e Z_\alpha^2 e^4 \ln\Lambda^{\alpha/e}}{4\pi\varepsilon_0^2 m_f^2}, \tag{21}$$

where Z_{eff} is the effective charge number of background ions, Z_α is the charge number of fast ions.

4.4 Derivation of the critical velocity of fast ions

The velocity of the fast ions from NBI is much larger than the thermal velocity of ions but still much smaller than the electron thermal velocity, i.e,

$$v_{ti} \ll v_f \ll v_{te}. \tag{22}$$

[For the 3.5MeV α particles created by D-T reaction in ITER plasmas, the relation in Eq. (22) also applies. The ratio of α particle's velocity to v_{te} is given by

$$\frac{v_\alpha}{v_{te}} = \sqrt{\frac{T_\alpha}{T_e} \frac{m_e}{m_\alpha}}. \tag{23}$$

For an electron temperature $T_e = 20\text{keV}$, the above equation gives

$$\frac{v_\alpha}{v_{te}} = \sqrt{\frac{3.5 \times 10^6 \text{eV}}{20 \times 10^3 \text{eV}} \frac{1}{1836}} = 0.304, \tag{24}$$

which indicates that the velocity of α particles are still smaller than the electron thermal velocity.] The collision friction encountered by the fast ions is a function of their velocity. The critical velocity of fast ions is the velocity for which the collision friction of the fast ions with electrons and ions is equal. Next, we derive the critical velocity. The collision friction coefficient due to an isotropic background distribution is given by[4]

$$F^{a/b}(v) = -\frac{4\pi\Gamma^{a/b}}{3n_b} \frac{m_a}{m_b} \frac{1}{v^2} \int_0^v 3(v')^2 f_b(v') dv', \tag{25}$$

where $\Gamma^{a/b}=\frac{n_b q_a^2 q_b^2}{4\pi\epsilon_0^2 m_a^2}\ln\Lambda^{a/b}$. Consider the collision friction of fast ions with thermal ions. Assume the distribution of the thermal ions are Maxwellian, then Eq. (25) is written

$$F^{f/i}(v)=-\frac{4\pi\Gamma^{f/i}}{3n_i}\frac{m_f}{m_i}\frac{1}{v^2}\int_0^v 3(v')^2 f_{Mi}(v')dv', \tag{26}$$

where

$$f_{Mi}=n_i\left(\frac{m_i}{2\pi T_i}\right)^{3/2}\exp\left(-\frac{v^2}{v_{ti}^2}\right), \tag{27}$$

with $v_{ti}=\sqrt{2T_i/m_i}$. Since v_f is much larger than the thermal velocity of ions, the collision friction coefficients can be approximated by the high-velocity-limit (i.e. setting the upper limit of the integration to be $+\infty$), which gives

$$\begin{aligned} F^{f/i}(v) &= -4\pi\Gamma^{f/i}\frac{m_f}{m_i}\frac{1}{v^2}\left(\frac{m_i}{2\pi T_i}\right)^{3/2}v_{ti}^3\frac{\sqrt{\pi}}{4} \\ &= -\Gamma^{f/i}\frac{m_f}{m_i}\frac{1}{v^2} \end{aligned} \tag{28}$$

For the collision friction of fast ions with thermal electrons, since $v_f \ll v_{te}$, Eq. (25) is written

$$\begin{aligned} F^{f/e} &= -\frac{4\pi\Gamma^{a/e}}{n_e}\frac{m_a}{m_e}\frac{1}{v^2}\int_0^v (v')^2 f_{Me}(v')dv' \\ &= -\frac{4\pi\Gamma^{a/e}}{n_e}\frac{m_a}{m_e}\frac{1}{v^2}\int_0^v (v')^2 n_e\left(\frac{m_e}{2\pi T_e}\right)^{3/2}\exp\left(-\frac{v^2}{v_t^2}\right)dv' \\ &= -4\pi\Gamma^{a/e}\left(\frac{m_e}{2\pi T_e}\right)^{3/2}\frac{m_a}{m_e}\frac{v_t^3}{v^2}\int_0^x x^2\exp(-x^2)dx, \end{aligned} \tag{29}$$

where $x=v/v_{te}$. Since $x\ll 1$, we expand $e^{-x^2}\approx 1$. Using this, Eq. (29) is written

$$\begin{aligned} F^{f/e} &= -4\pi\Gamma^{f/e}\left(\frac{m_e}{2\pi T_e}\right)^{3/2}\frac{m_f}{m_e}\frac{v_{te}^3}{v^2}\int_0^x (x^2)dx \\ &= -4\pi\Gamma^{f/e}\left(\frac{m_e}{2\pi T_e}\right)^{3/2}\frac{m_f}{m_e}\frac{v_{te}^3}{v^2}\left(\frac{x^3}{3}\right) \\ &= -4\pi\Gamma^{f/e}\left(\frac{m_e}{2\pi T_e}\right)^{3/2}\frac{m_f}{m_e}\frac{v}{3} \end{aligned} \tag{30}$$

The critical velocity $v_{\rm crit}$ is the velocity for which $F^{f/i}$ and $F^{f/e}$ are equal to each other, i.e. $F^{f/i}=F^{f/e}$. Using this, along with Eqs. (28) and (30), we obtain

$$-\Gamma^{f/i}\frac{m_f}{m_i}\frac{1}{v_{\rm crit}^2}=-4\pi\Gamma^{f/e}\left(\frac{m_e}{2\pi T_e}\right)^{3/2}\frac{m_f}{m_e}\frac{v_{\rm crit}}{3}, \tag{31}$$

Noting that $\Gamma^{a/b}=\frac{n_b q_a^2 q_b^2}{4\pi\epsilon_0^2 m_a^2}\ln\Lambda^{a/b}$ and $\ln\Lambda^{f/i}\approx\ln\Lambda^{f/e}$, and

$$\frac{\Gamma^{f/i}}{\Gamma^{f/e}}=\frac{n_i Z_i^2}{n_e}\equiv Z_{\rm eff} \tag{32}$$

equation (31) is written

$$v_{\rm crit}=\left(Z_{\rm eff}\frac{m_e}{m_i}\frac{3\sqrt{\pi}}{4}\right)^{1/3}v_{te},$$

which corresponds to the fast ions kinetic energy

$$E_{\rm crit}\equiv\frac{1}{2}m_f v_{\rm crit}^2=\frac{m_f}{m_i}\left(\frac{m_i}{m_e}\right)^{1/3}\left(Z_{\rm eff}\frac{3\sqrt{\pi}}{4}\right)^{2/3}T_e, \tag{33}$$

which agrees with the critical energy given in Ref. [6] ($Z_{\rm eff}=1$ is assumed in Ref. [6]). Recall that the beam velocity is assumed to be in the range given by Eq. (22), i.e., $v_{ti}\ll v_f\ll v_{te}$. In this range, $F^{f/e}\propto v_f$ while $F^{f/i}\propto 1/v_f^2$. Thus, if $v_f>v_{\rm crit}$, then the collision friction of the beam ions with the background electrons will exceed the friction with the background ions, so that the beam ions will mainly heat electrons.

4.5 Slowing-down time of energetic particles

For energetic particles whose energy is larger than the critical energy, the collision friction is dominated by the friction with the background electrons. The collision friction coefficient with the electrons is then given by Eq. (30), i.e.,

$$F^{f/e} = -4\pi\Gamma^{f/e}\left(\frac{m_e}{2\pi T_e}\right)^{3/2}\frac{m_f}{m_e}\left(\frac{v}{3}\right) \tag{34}$$

The slowing down time t_s is defined by

$$t_s = \frac{v}{|F|}, \tag{35}$$

which, by using Eq. (34), is written

$$t_s = \frac{3\sqrt{2\pi}T_e^{3/2}}{\frac{n_e Z_f^2 e^4}{2\pi\epsilon_0^2 m_f^2}\ln\Lambda^{f/e}}\frac{1}{\sqrt{m_e}m_f}. \tag{36}$$

Equation (36) agrees with the slowing down time given in Ref. [6] (the formula after Eq. (1) of Ref. [6]). Note that the slowing down time t_s increase with the increasing of T_e, but decrease with the increasing of n_e. Also note that the slowing down time given by Eq. (36) is independent of the velocity of fast ions. For EAST parameters $T_e = 2\text{keV}$, $n_e = 4\times10^{19}m^{-3}$, the slowing down time of a fast Deuterium ion calculated by Eq. (36) is $t_s = 565\text{ms}$. However, the velocity of fast ions form 80keV NBI on EAST is in the vicinity of the critical velocity, for which the friction of fast ions with the thermal ions should be taken into account. Therefore, the more accurate value of slowing down time on EAST is much shorter than the 565ms given above, e.g. 100ms.

5 RMP field

The Biot-Savart law for an idealized zero-thinkness wrie is given by

$$\mathbf{B}(\mathbf{r}) = \frac{\mu_0}{4\pi}\int\frac{\mathbf{I}(\mathbf{r}')\times(\mathbf{r}-\mathbf{r}')}{|\mathbf{r}-\mathbf{r}'|^3}dl \tag{37}$$

$$= \frac{\mu_0}{4\pi}\int I(\mathbf{r}')\frac{d\mathbf{l}(\mathbf{r}')\times(\mathbf{r}-\mathbf{r}')}{|\mathbf{r}-\mathbf{r}'|^3}, \tag{38}$$

where $I(r)$ is the current flowing in the wire, $d\mathbf{l}(\mathbf{r}')$ is an line element along the wire.

$$\mathbf{r}-\mathbf{r}' = (x-x')\hat{\mathbf{e}}_x + (y-y')\hat{\mathbf{e}}_y + (z-z')\hat{\mathbf{e}}_z \tag{39}$$

5.1 For wires on poloial plane

For a coil on a poloidal plane, $d\mathbf{l}$ is written as $d\mathbf{l} = dZ\hat{\mathbf{e}}_z + dR\hat{\mathbf{e}}_R(\phi)$. In Cartesian coordinates, $d\mathbf{l}$ can be written as

$$d\mathbf{l} = dR\cos\phi\hat{\mathbf{e}}_x + dR\sin\phi\hat{\mathbf{e}}_y + dZ\hat{\mathbf{e}}_z \tag{40}$$

Using Eq. (40) and (39), we obtain

$$d\mathbf{l}\times(\mathbf{r}-\mathbf{r}') = \begin{vmatrix} \hat{\mathbf{e}}_x & \hat{\mathbf{e}}_y & \hat{\mathbf{e}}_z \\ dR\cos\phi & dR\sin\phi & dZ \\ (x-x') & (y-y') & (z-z') \end{vmatrix}$$

5.2 For wires along toroidal direction

$$d\mathbf{l} = Rd\phi\hat{\mathbf{e}}_\phi = Rd\phi(-\sin\phi\hat{\mathbf{e}}_x + \cos\phi\hat{\mathbf{e}}_y) \tag{41}$$

Using Eq. (41) and (39), we obtain

$$d\mathbf{l}\times(\mathbf{r}-\mathbf{r}')=\begin{vmatrix} \hat{\mathbf{e}}_x & \hat{\mathbf{e}}_y & \hat{\mathbf{e}}_z \\ -Rd\phi\sin\phi & Rd\phi\cos\phi & 0 \\ (x-x') & (y-y') & (z-z') \end{vmatrix} \tag{42}$$

Appendix A Ionization cross section given in Wesson's book

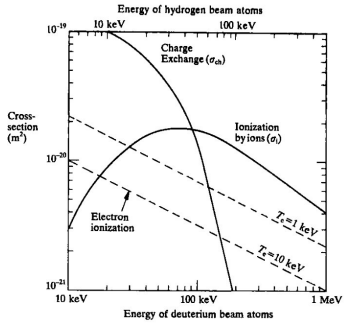

Figure 27. Fig. 5.3.1 of Wesson's book "Tokamaks", which shows the cross-sections for charge exchange and ionization by plasma ions and the effective cross-section for ionization by electrons, as functions of the energy of neutral beam atoms.

Bibliography

[1] O. Demokan and V. Mirnov. Rigorous treatment of charge exchange, ionization, and collisional processes in neutral-beam-injected mirrors. *Physics of Plasmas*, 2(1):139–145, 1995.

[2] R. K. Janev and J. J. Smith. Cross sections for collision processes of hydrogen atoms with electrons, protons and multiply charged ions. *Atomic and Plasma-material Interaction Data for Fusion*, 4, 1993.

[3] Igor D. Kaganovich, Edward A. Startsev, and Ronald C. Davidson. Scaling cross sections for ion-atom impact ionization. *Physics of Plasmas*, 11(3):1229–1232, 2004.

[4] Charles F. F. Karney. Fokker-planck and quasilinear codes. *Comp. Phys. Rep.*, 4:183–244, 1986.

[5] Z. Lin, W. M. Tang, and W. W. Lee. Gyrokinetic particle simulation of neoclassical transport. *Physics of Plasmas*, 2(8):2975, 1995.

[6] ITER physics basis editors. Chapter 5: physics of energetic ions. *Nucl. Fusion*, 39(12):2471, 1999.

[7] Y. Todo, M.A. Van Zeeland, A. Bierwage, and W.W. Heidbrink. Multi-phase simulation of fast ion profile flattening due to alfvén eigenmodes in a diii-d experiment. *Nucl. Fusion*, 54(10):104012, 2014.